Electronic Supplementary Material (ESI) for RSC Advances
This journal is © The Royal Society of Chemistry 2014

Controllably oxidized copper flakes as multicomponent copper-based catalysts for Rochow reaction

Shaomian Liu,[a,b] Yingli Wang,[b] Yongxia Zhu,[b] Guangna Wang,[b]

Zailei Zhang,[b] Hongwei Che,[c] Lihua Jia,[*,a] and Fabing Su[*,b]

[a] *College of Chemistry and Chemical Engineering, Qiqihaer University, Qiqihaer, Heilongjiang Province, China 161006*

[b] *State Key Laboratory of Multiphase Complex Systems, Institute of Process Engineering, Chinese Academy of Sciences, Beijing, China 100190*

[c] *College of Equipment Manufacturing, Hebei University of Engineering, Hebei province, China 056038*

*To whom correspondence should be addressed. E-mail address: jlh29@163.com (L. Jia), fbsu@mail.ipe.ac.cn (F. Su), Tel.: +86−10−82544850, Fax: +86−10−82544851.

This journal is © The Royal Society of Chemistry 2014

Abstract

The metallic Cu flakes prepared by milling metallic Cu powder were controllably oxidized in air at different temperatures to obtain the Cu-based catalysts containing multicomponent of Cu, Cu_2O, and CuO. These catalysts are explored in the Rochow reaction using silicon powder and methyl chloride (MeCl) as reactants to produce the dimethyldichlorosilane (M2), which is the most important organosilane monomer in the industry. The samples were characterized by X-ray diffraction, temperature-programmed reduction, thermogravimetric analysis, oxidimetry analysis, particle size analysis, transmission electron microscopy, and scanning electron microscopy. Compared to the metallic Cu powder and Cu flakes, the controllably oxidized Cu flakes containing Cu, Cu_2O, and CuO species show much higher M2 selectivity and silicon conversion in the Rochow reaction. The enhanced catalytic performance may stem from the larger interfacial contact among the gas MeCl, solid Si particles, and solid Cu-based catalyst flakes, as well as the synergistic effect among the different Cu species. The work would be helpful to the development of novel Cu-based catalysts for organosilane synthesis.

This journal is © The Royal Society of Chemistry 2014

1. Introduction

The flaky metals such as Al,[1] Ni,[2] Zn,[3] Au,[4] Cu,[5, 6] and alloy,[7, 8] which are generally produced by ball milling in industry,[1] are widely applied in electrode material,[5, 9] pigment,[3, 10] and catalysts.[11] This is because of their two-dimension structural characteristics, which endow these materials with some special properties, such as good adhesive ability,[10, 12] excellent conductivity,[5, 9] strong light reflection[3, 10] and commendable catalytic performance.[11, 13] It is known that the catalytic performance of a heterogeneous catalyst is strongly affected by contact area between reactants and metal catalysts with a specific morphology and/or small particle size. Compared with the bulk counterparts, the metal flaks with even the same volume normally have much more active surface, thus conducive to catalysis.

The Rochow reaction, which was discovered in 1940s,[14] is commercially employed to produce methylchlorosilanes (MCSs). In this reaction, gas methyl chloride (MeCl) reacts with solid silicon (Si) powder in the presence of Cu-based catalysts and a trace amount of promoters as following Formula 1:[15]

$$\mathrm{Si} + \mathrm{MeCl} \xrightarrow[300\text{-}350\ ^{o}\mathrm{C}]{\text{copper catalyst}} \begin{array}{l}(CH_3)_3SiCl\\(CH_3)_2SiCl_2\\CH_3SiCl_3\\CH_3HSiCl_2\\(CH_3)_2HSiCl\\\text{other low boilers}\\\text{residue}\end{array} \qquad (1)$$

Among the products from the above Rochow reaction, dimethyldichlorosilane ($(CH_3)_2SiCl_2$, M2) is the most important monomer used for silicon rubber in organosilane industry, and thus a high M2 yield is the most desired. Besides the accurate control of reaction conditions and selection of proper reactors, the development of highly efficient Cu-based catalyst is critical for a high M2 selectivity and Si conversion. It has been reported that Cu-based catalysts, including metallic Cu,[14, 16] Cu_2O,[17,

This journal is © The Royal Society of Chemistry 2014

[18] CuO,[17] CuCl,[19, 20] Cu-Si alloy,[21, 22] and Cu-Cu_2O-CuO,[23] are active in the presence of promoter additives.[24-26] In organosilane industry, the Cu-based catalysts containing Cu, Cu_2O, and CuO prepared via high-energy mechanical milling have been widely applied.[23] Recently, various cupreous and copper oxide structures, including flower-like ZnO grown on urchin-like CuO microsphere,[25] porous cubic Cu microparticle,[27] mesoporous Cu_2O microsphere,[28] shape-controlled Cu_2O microparticle,[29] dandelion-like CuO microsphere,[30] flower-like CuO microsphere,[31] CuCl microcrystal with different morphologies,[32] and Cu@Cu_2O core-shell microsphere,[33] have been developed in our group as model Cu-based catalysts to explore the catalytic properties for M2 synthesis. It is found that surface morphology, pore structure, particle size, and catalyst composition have significant effects on the Rochow reaction. However, all the above Cu-based catalysts are always in the micrometer size and the synergistically catalytic effect between different components is not fully understood yet. More recently, Liu et al.,[34] prepared nanosized Cu-based catalysts with multicomponent of Cu, Cu_2O, and CuO by partial reduction of CuO nanoparticles in hydrogen. However, a large scale manufacture of such catalysts seems impossible considering the preparation cost. On the other hand, these nanosized catalysts are hardly stored for a long time due to the easy surface oxidation of the reduced Cu nanoparticles when exposed to air. As we know, the oxidation of Cu could generate surface copper oxide film, which may avoid above problems. In addition, metallic Cu and alloyed Cu flakes have been used in laboratory for MCS synthesis.[16] Combining these ideas, it is expected to generate flaky multicomponent Cu-Cu_2O-CuO catalysts via partially oxidation of the Cu flake as Cu-based catalysts for the Rochow reaction.

Herein, we report the preparation of partially oxidized Cu flake as Cu-based catalysts for the Rochow reaction by dry milling and controllable oxidation processes. These catalysts can be easily scaled up in industry. Compared with metallic Cu powder and Cu flakes, the controllably oxidized

This journal is © The Royal Society of Chemistry 2014

Cu flakes containing Cu, Cu_2O, and CuO species show much higher M2 selectivity and Si conversion because of the improved contact between catalyst particles and Si powders, and the synergistic effect among different Cu species. Our work would be helpful for developing novel Cu-based catalysts.

2. Experimental

2.1. Material synthesis

20.0 g of Cu powders (denoted Cu-p, C. P., Beijing General Research Institute of Mining & Metallurgy, China) and 2.0 wt. % of stearic acid ($C_{18}H_{36}O_2$, C.P., Shijiazhuang Xinghong Rubber and Plastic Additives Sales Co, Ltd., China)[35] were mixed and mechanically ball-milled for 2 h in a planet-ball-grinding machine (QM-3SP04, Nanjing NanDa Instrument Plant, China). The milling process was carried out at 600 rpm in a Teflon container using 8 mm diameter stainless steel balls with ball-to-powder weight ratio of 30:1. The obtained Cu flake powders were denoted Cu-f. In the oxidation process, 10.0 g of Cu-f was placed in a square crucible, which was then put in a corundum tube in a tube furnace. The samples were oxidized in air (50.0 mL/min) with ramp rate of heating at 5 ^oC/min at different temperatures of 200, 300, 400, and 500 ^oC for 10 min, naturally cooled down to room temperature in a pure N_2 flow, and were denoted Cu-Cu_2O-f, Cu-Cu_2O-CuO-f, Cu_2O-CuO-f, and CuO-f, respectively.

2.2. Characterization.

X-ray diffraction (XRD) analysis were performed with a PANalytica X'Pert PRO MPD using the Kα radiation of Cu (λ = 1.5418 Å) and checked with the card number of Joint Committee on Powder Diffraction Standards (JCPDS). The crystallite size was calculated using the Debye-Scherrer equation. The microscopic feature of the sample was observed by field-emission

This journal is © The Royal Society of Chemistry 2014

scanning electron microscopy (SEM) (JSM-7001F, JEOL, Tokyo, Japan) with energy-dispersive spectroscopy (EDS) (INCA X-MAX, JEOL, Oxford, England) and transmission electron microscopy (TEM) (JEM-2010F, JEOL, Tokyo, Japan). Thermogravimetric (TG) analysis was carried out on an EXSTAR TG/DTA 6300 (Seiko Instruments, Japan) with a heating rate of 5.0 ^{o}C/min in air (200 mL/min). H_2-temperature programmed reduction (TPR) measurements were carried out on an automated chemisorption analyzer (ChemBET pulsar TPR/TPD, Quantachrome). Upon loading of about 0.1 g of sample into a quartz U-tube, the samples was degassed at 150 ^{o}C for 30 min under helium. When the temperature was dropped to 30 ^{o}C, the gas was changed to 9.9 % H_2/He. Finally, the sample was heated from 30 to 900 ^{o}C at 10 ^{o}C/min under the H_2/He flow (30 mL/min). The Particle size distribution (PSD) was measured by Laser Particle size analyzer (BT-9300Z, Bettersize Instruments Ltd., China). 1.0 g sample was added to sample cell containing deionized water. After 3 min of in-situ ultrasonication, the PSD data and curve were automatically given. Oxidimetry analysis was used for determine the content of Cu, Cu_2O, and CuO components within a sample. All used chemicals with an analytical grade were purchased from Sinopharm Chemical Reagent Co., Ltd. China. A sample of 0.3 g was putted into a flask containing 120.0 mL acetonitrile (CH_3CN, 95 %), followed by adding 40.0 mL of 18.5 w % diluted HCl to form a mixture. After vigorously rocking for 20 seconds and immediate filtration, 160.0 mL deionized water was added to the filtrated solution and then titrated with 0.02 mol/L $KMnO_4$ (≥99.5 %). The content of Cu_2O in the sample can be calculated by the amount of consumed $KMnO_4$ (Formula 2). The residual solid precipitate after above filtration was dissolved in 20.0 mL of 0.1 mol/L $FeCl_3$ solution kept at 50 ^{o}C in water bath, and then cooled down to room temperature (Formula 3). The solution was added with 20.0 mL of 0.7 mol/L $MnSO_4$ solution and 100.0 mL deionized water, and again titrated with 0.02 mol/L $KMnO_4$ solution. The content of Cu is further calculated through the

This journal is © The Royal Society of Chemistry 2014

amount of ferrous iron derived from amount of consumed $KMnO_4$ (Formula 4). The content of CuO is thus the result of total amount of sample subtracting the amount of Cu and Cu_2O.

$$8H^+ + 5Cu^+ + MnO_4^- \rightarrow 5Cu^{2+} + Mn^{2+} + 4H_2O \quad (2)$$

$$Cu + 2Fe^{3+} \rightarrow Cu^{2+} + 2Fe^{2+} \quad (3)$$

$$8H^+ + 5Fe^{2+} + MnO_4^- \rightarrow 5Fe^{3+} + Mn^{2+} + 4H_2O \quad (4)$$

2.3. Catalytic measurement

The evaluation of catalyst was carried out with a typical MCS lab fixed-bed reactor. 10.0 g of Si powder (20−50 mesh, provided by Jiangsu Hongda New Material Co., Ltd.) and 1.0 g of prepared product catalyst together with 0.1 g of Zinc (Zn, A.R., Sinopharm Chemical Reagent Co., Ltd.) used as a promoter were homogeneously mixed to form a contact mass, which was loaded in the glass reactor. The reactor system was purged with purified N_2 for 0.5 h followed by heating to 325 ^oC within 1 h under a N_2 flow rate of 25 mL/min. Subsequently, N_2 was turned off, and MeCl gas with a flow rate of 25 mL/min was introduced into the reactor to react with Si followed by heating to 325 ^oC. After a given period of 24 h, the reaction was stopped. The gas product was cooled into liquid phase with the circulator bath controlled at 5 ^oC by a programmable thermal circulator (GDH series, Ningbo Xinzhi Biological Technology Co., Ltd., China). The products in the liquid solution were quantitatively analyzed on an Agilent Technologies gas chromatograph (GC-7890A) equipped with a KB-210 column (60 m) and a TCD detector. Gas chromatography System was used for identification of the products, which was mainly comprised of methyltrichlorosilane (CH_3SiCl_3, M1), M2, trimethylchlorosilane ($(CH_3)_3SiCl$, M3), methyldichlorosilane (CH_3SiHCl_2, M1H), dimethylchlorosilane ($(CH_3)_2SiHCl$, M2H), low boiler (LB) and high boiler (HB). The selectivity of the products was calculated by the peak area ratio (in percentage). The waste contact mass (residual solid after reaction) containing unreacted Si powder, Cu compounds, and promoters were weighed

This journal is © The Royal Society of Chemistry 2014

to calculate Si conversion, which was that the ratio of weight difference of contact mass (before and after reaction) and weight of Si (before reaction) (Formula 5).

$$\textbf{Conversion of Si } (C_{Si}) = \frac{\textbf{weight}_{\text{contact mass before reaction}} - \textbf{weight}_{\text{contact mass after reaction}}}{\textbf{weight}_{\text{Si before reaction}}} \times 100\,\% \quad (5)$$

3. Results and discussion

3.1. Characterization

Fig. 1a shows the XRD patterns of all the samples. Diffraction peaks of Cu-p at 2θ values of 43.3, 50.5 and 74.2° are observed, which correspond to the lattice plane of (110), (200) and (220) of pure Cu phase (JCPDS No. 01-070-3039), respectively. Accordingly, the XRD pattern of Cu-f shows the same diffraction peaks as those in Cu-p but with broadened shape and decreased intensity, suggesting a degraded crystal structure, which is due to the decrease of grain size during milling [8]. For Cu-Cu_2O-f, two new peaks appeared at 2θ values of 36.7 and 42.7°, which correspond to the lattice planes of (111) and (200) of cubic Cu_2O (JCPDS No. 00-001-1142), respectively, suggesting the formation of a bi-component material of Cu and Cu_2O. The diffraction peaks of Cu-Cu_2O-CuO-f at 2θ values of 33.5, 35.5, 38.2, 48.7, 54.2, 58.3, 62.5, 66.4, 68.2, 73.4, and 75.6° are observed, which correspond to the lattice planes of (110), (−111), (111), (−202), (020), (202), (−113), (−311), (220), (311), and (111) of monoclinic CuO (JCPDS No. 03-065-2309), respectively. From Cu-Cu_2O-CuO-f to Cu_2O-CuO-f, the diffraction peaks of Cu are gradually weakened until completely disappeared with the increase of the oxidation temperature. Further increasing the temperature to 500 °C, the XRD pattern of CuO-f suggests the formation of pure CuO. The grain size of Cu, Cu_2O, and CuO in each sample was calculated based on the 2θ values of 35.8, 36.7, and 43.4 °, respectively, and compiled in Table 1, in which, it can be seen that the grain size of Cu in

This journal is © The Royal Society of Chemistry 2014

Cu-p is 32.5 nm, slightly larger than that in Cu-f (28.9 nm). In Cu-Cu_2O-f and Cu-Cu_2O-CuO-f, the grain size of Cu decreases gradually from 28.5 to 28.0 nm. This may because vacancies or vacancy clusters in Cu grain boundaries move easily along grain boundaries towards the surfaces and then disappear rapidly. As a result, the atomic arrangement tends fast towards an ordered arrangement, and thus the grain size of Cu becomes small, with the increasing oxidation temperature.[36, 37] The grain size of Cu_2O in Cu-Cu_2O-f, Cu-Cu_2O-CuO-f, and Cu_2O-CuO-f is 28.3, 34.3, and 39.7 nm, respectively. For Cu-Cu_2O-CuO-f, Cu_2O-CuO-f, and CuO-f, the grain size of CuO increases gradually from 38.3 to 54.7 nm with the increase of the oxidation temperature.[38, 39]

Fig. 1b shows the TG curves of all the samples measured in air. For Cu-p, the weight is gradually increased to about 24.5 wt% at 800 ^oC, close to the theoretical value (25.0 wt%), indicating the high purity of metallic Cu. For Cu-f, in the temperature range of 230−250 ^oC, a weight loss of 0.7 wt% close to the amount of residual stearic acid used in milling process can be attributed to its decomposition, which is confirmed by the TG analysis of pure stearic acid (not shown here). The weight increase of Cu-f is about 23.5 wt% at 800 ^oC, slightly less than its theoretical value (24.3 wt%) considering the presence of stearic acid in this sample. A similar weight loss in the temperature range of 230−250 ^oC is also seen for Cu-Cu_2O-f because its oxidation was carried out at 200 ^oC, less than the decomposition temperature of stearic acid. However, this weight loss disappeared when the oxidation temperature is beyond to 300 ^oC because stearic acid was decomposed during the oxidation process. For Cu-Cu_2O-f and Cu-Cu_2O-CuO-f, their weight increase is about 18.3 and 11.4 wt%, respectively, which is due to the oxidation of Cu and Cu_2O to CuO, in good agreement with the values calculated based on the oxidimetry result (18.5 and 11.7 wt%). For Cu_2O-CuO-f, the weight increase derived from the oxidation of Cu_2O to CuO is 4.2 wt%, and thus the calculated Cu_2O content in this sample is about 38.8 wt%, consistent with the

This journal is © The Royal Society of Chemistry 2014

oxidimetry result (39.1 wt% in Table 1). It is seen that there is no visible weight change for sample CuO-f, suggesting it is nearly pure CuO.

Fig. 1c shows the H_2-TPR profiles of all the samples. The hydrogen consumption peak areas and peak temperatures (T_M) are compiled in Table 1. It can be seen that, with the increase of the CuO content in the samples (Cu-Cu_2O-f, Cu-Cu_2O-CuO-f, Cu_2O-CuO-f, and CuO-f), the reduction temperature is slightly decreased but the hydrogen consumption is increased. For the oxidized samples, the reduction peaks move forward to a slightly lower temperature region with the increase of the oxidation temperature. This may be because of the formation of more defects in the oxidized products at a higher temperature.[40] Using the ratio of hydrogen consumption peak area to the mole number of O in CuO-f as the reference and based on the above TG analysis, it can calculate that the content of CuO in Cu-Cu_2O-CuO-f and Cu_2O-CuO-f samples are about 60.4 and 31.1 wt%, respectively, in good agreement with the above oxidimetry result (60.9 and 31.2 wt% in Table 1). For Cu-Cu_2O-f, the content of Cu_2O is 46.7 wt%, consistent with the oxidimetry result (47.0 wt% in Table 1). Therefore, the contents of Cu, Cu_2O, and CuO within the products can be well tuned by controlling the oxidation temperature. Fig. 1d shows the PSD curves of all the samples. The median diameter of Cu-p, Cu-f, Cu-Cu_2O-f, Cu-Cu_2O-CuO-f, Cu_2O-CuO-f, and CuO-f at the maximum peak position is 31.2, 21.7, 20.7, 20.4, 20.2, and 17.5 μm, indicating the particle size is slightly decreased with the increase of the oxidation temperature, which may be caused by different levels of damage and dislocation during the oxidation process, resulting in more defects which may be active for the Rochow reaction. [23]

Fig. 2a and 2b present the SEM images of the Cu-p, which show the branch-like morphology with a wide size range of 30−120 μm. The SEM images of Cu-f in Fig. 2c and 2d show that the Cu-f flakes with a narrow flake diameter range of 40−80 μm have a smooth surface and a uniform flaky

This journal is © The Royal Society of Chemistry 2014

structure with a thickness between 0.5 and 0.8 μm. The flake diameter of Cu-Cu_2O-f (Fig. 2e-2l), Cu-Cu_2O-CuO-f (Fig. 2g-2h), Cu_2O-CuO-f (Figure 2i-2j), and CuO-f (Fig. 2k-2l) is around 40−80 μm, similar to that of Cu-f. The morphology of Cu-Cu_2O-f has no significant difference from that of Cu-f, but the surface of Cu-Cu_2O-CuO-f shows a grain-like appearance and Cu_2O-CuO-f has a blade-like structure. Furthermore, the surface of CuO-f exhibits a clear ruffle-like microstructure after a higher oxidation temperature (500 ^oC), which is generated from the full introduction of oxygen and may indicate that oxidation of CuO-f is well processed.

Fig. 3 shows the TEM images of all the flaky samples. It is seen that the lattice plane distance of Cu-f is 0.21 nm (Fig. 3a), corresponding to the (111) plane distance of cubic Cu derived from the XRD pattern. The TEM image of Cu-Cu_2O in Fig. 3b shows the presence of two different lattice plane distances of 0.21 and 0.24 nm, corresponding to that of Cu (111) and Cu_2O (111) respectively. Similarly, Cu-Cu_2O-CuO-f (Fig. 3c) has three lattice plane distances of 0.21, 0.24, and 0.25 nm, corresponding to that of Cu (111), Cu_2O (111), and CuO (−111), respectively. In Cu_2O-CuO-f (Fig. 3d), there are two lattice plane distances of 0.24 and 0.25 nm, corresponding to that of Cu_2O (111) and CuO (−111), respectively. For CuO-f (Fig. 3e), the lattice plane distance is around 0.25 nm, indicating the presence of CuO (−111). These results suggest that the prepared Cu-based samples are composed of polycrystals while each multi-component particle consists of different Cu component crystals.

3.2. Controllable oxidation mechanism

The oxidation process of Cu flakes is proposed as depicted in Fig. 4. In the oxidation process, it is normally accepted that copper oxidation involves the migration of electrons and cations to the reaction zone.[41] It hypothesizes that a very strong electric field is set up through the oxide between

This journal is © The Royal Society of Chemistry 2014

the Cu and the absorbed O at the gas interface, which enables the Cu ions to move through the oxide to the reaction zone (Formulas 6 and 7). The possible oxidation steps are shown as the following equations:

$$Cu \rightarrow Cu^{+} + e^{-} \quad (6)$$

$$O_2 \rightarrow O + O \quad (7)$$

$$2Cu^{+} + O + 2e^{-} \rightarrow Cu_2O \quad (8)$$

$$Cu_2O + O \rightarrow 2CuO \quad (9)$$

For Cu-Cu_2O-f, it is generally believed that cuprous oxide accounts predominantly for the adherent layer formed below 250 ^{o}C (Fig. 4a). In this process, the transfer of Cu ions actually occurs by the formation of vacant cationic sites at the metal-oxide interface, followed by their diffusion to the oxide-oxygen interface.[42] The external-oxide scale formed on a Cu surface grows at the scale-gas interface by outward Cu-ion diffusion (Formulas 8 and 9). Two copper oxides (Cu_2O and CuO) are stable in the copper-oxygen system.[43] In the temperature range of 250−350 ^{o}C, the values reported for the relative amounts of cuprous and cupric oxides show large discrepancies. Grain grown on Cu is oxidized at 300 ^{o}C, in which Cu oxidation is contributed from lattice diffusion and grain boundary diffusion. The rate-determining step in this temperature range is the outward diffusion of Cu in Cu_2O. The same process is also suitable to the description of formation of Cu-Cu_2O-CuO-f (Fig. 4b). For the formation of CuO on Cu_2O during oxidation, it is believed that the growth of Cu_2O is predominant at 350−500 ^{o}C, which are attributable to the predominant growth of Cu_2O by outward diffusion of Cu cations, just as the grain boundary diffusion does at 350−500 ^{o}C. For Cu_2O-CuO-f, fast grain boundary diffusion in the high range of temperature leads to blade growth on Cu oxidized at 400 ^{o}C. Oxide blades grow predominantly by surface diffusion of cations along a tunnel centered on the core of a dislocation (Fig. 4c). For CuO-f, the lattice diffusion

This journal is © The Royal Society of Chemistry 2014

contributes to Cu oxidation at high temperatures. Thus, as the temperature increases, lateral lattice diffusion becomes relatively more favorable, and oxide growth leads to a ruffle-like microstructure. As there are some residues of Cu cations, which penetrate the Cu_2O lattices following the layer-by-layer fashion from inner to outside, ultimately, Cu_2O is converted to CuO completely (Fig. 4d). The composition of the superficial oxide layer on Cu undergoes large variations over the temperature range of 0−500 ^oC.[44] As explained, lattice, grain boundary, and surface diffusion can contribute to the surface growth of oxide grain, blade and ruffle-like microstructure in the oxidation process. Therefore, by turning the temperature, it is able to control the content of Cu, Cu_2O, and CuO, and the surface morphology for the Cu-based catalysts.

3.3 Catalytic Property.

Table 2 shows the catalytic performance of all the samples as model Cu-based catalysts for M2 synthesis via the Rochow reaction. It can be seen that the M2 selectivity and Si conversion of Cu-p is 5.7 and 1.6 %, respectively, while that of Cu-f increases to 54.0 and 16.3 %, respectively. This is because the flake structure and higher surface area of Cu-f offer better contact between the catalysts and the Si powders,[11] which can improve the catalytic property. For Cu-Cu_2O-f, the M2 selectivity and Si conversion rises up to 62.5 and 24.8 %, respectively, and more importantly, Cu-Cu_2O-CuO-f shows much increased values of 82.0 and 32.4 % in the first test (its values are reproducible during 3 tests), respectively, higher than those of Cu_2O-CuO-f (80.1% M2 selectivity and 30.7% Si conversion). For CuO-f, both M2 selectivity and Si conversion decrease slightly. These results demonstrate that the prepared catalysts possessing three components of Cu, Cu_2O, and CuO have the best catalytic performance among all the samples tested possibly because of the synergistic effect among Cu, Cu_2O, and CuO, which promotes the catalytic activity for the Rochow reaction.[33]

This journal is © The Royal Society of Chemistry 2014

The byproducts such as M1, M3, M1H, M2H, LB, and HB without a big difference over the various prepared catalysts are also detected in the products.

Fig. 5 displays the XRD patterns of the waste contact masses after reaction, which is the solid mixture of the unreacted Si, the Cu-based catalyst, and trace promoter Zn. After the reaction, all the waste contact masses are composed of Si and Cu, but no Cu_2O and CuO species are detected in Fig. 5a. The formation of Cu may originate from the reaction of MeCl with the lattice oxygen of the Cu-based catalyst.[17] An enlarged view of the XRD patterns in the range of 40−50^o (Fig. 5b) shows the presence of Cu_3Si and $Cu_{6.69}Si$ species, suggesting the formation of alloyed Cu_xSi active components through reaction of Cu and Si via diffusion during the reaction. In the Rochow reaction, Cu_3Si is normally suggested as the key catalytic active species,[45, 46] by which MCSs, especially M2, are formed. Cu_3Si is normally created between the Cu catalyst and the Si interface at elevated temperatures.[18] The amounts of Cu_3Si can substantially affect the Si conversion and M2 selectivity.[19] Although the intensity of Cu peaks for all the waste contact masses are almost similar, a much higher intensity of Cu_xSi is observed for Cu-Cu_2O-CuO-f than the other samples, suggesting that Cu-Cu_2O-CuO-f is more active in generating Cu_xSi than the other samples. This may be due to the proper ternary composition of Cu-Cu_2O-CuO flakes which creates a stronger synergistic effect and more contacts between the catalysts and the solid Si, thus promoting the formation of active Cu_xSi phases, which is the key step to enhance the catalytic activity for M2 production.

Fig. 6a shows the SEM images of the Si particles after the reaction using Cu-Cu_2O-CuO-f as the catalyst. It can be seen that the smooth region on the surface of Si particle stems from the unreacted Si, and coarse or cavity-like region is from reacted Si, suggesting the occurrence of etching process during the reaction, consistent with the so-called anisotropic etching reaction mechanism.[28] The element mapping images show the distribution of the elements Si (Fig. 6b) and Cu (Fig. 6c) on the

surface of the waste contact mass. The element Si image clearly shows reacted (dark yellow) and unreacted (bright yellow) zones of Si particle. Similarly, the element Cu image presents a uniform distribution on the reacted or etched Si surface, suggesting the occurrence of catalytic reaction between Si particles and Cu-based catalysts. Thus, the Rochow reaction can be schematically illustrated in Fig. 6d. In the process, a large quantity of silicon is fully mixed with a small quantity of partially oxidized Cu flakes before the reaction. With Cu diffusing into the Si matrix, the Cu_xSi alloy is gradually formed between the Cu catalyst and the Si interface with the elevated temperatures. In the reaction the bulk solid phase presented at reacting surface regions of silicon particles is Cu_xSi, which is reacted with the gas MeCl to form MSCs. As the reaction proceeds, more element copper is produced while the Cu in the Cu_xSi alloy is reduced until the deactivated stage. Clearly, the presence of the flake structure enhances the gas diffusion into the Cu-Si contact area, leading to the formation of much more active species. However, it should be noted that the real synergistic effect is not yet fully understood and should be further explored. In this work, we tentatively explored the effect of Cu-based catalysts with the flaky structure on catalytic property for the Rochow reaction. Following this method, more efficient Cu-Cu_2O-CuO flaky catalysts could be successfully developed.

4. Conclusions

In summary, we have demonstrated that the multicomponent flaky Cu-based catalysts with variable Cu, Cu_2O and CuO contents can be prepared by the dry grinding technology followed with controlled oxidation. Compared with metallic Cu powder and flakes applied in M2 synthesis via the Rochow reaction, the multicomponent Cu-based catalyst shows much higher M2 selectivity and Si conversion, proving the significance of the morphological structure and multicomponent contents in

This journal is © The Royal Society of Chemistry 2014

the catalytic properties. Our work would be very helpful in designing more efficient Cu-based catalysts and understanding the catalytic mechanism for the Rochow reaction.

Acknowledgments

The authors gratefully acknowledge the financial supports from the National Natural Science Foundation of China (Nos. 21206172, 21206025 and 51272252).

This journal is © The Royal Society of Chemistry 2014

References

1 S. H. Hong, D. W. Lee and B. K. Kim, *J. Mater. Process. Technol.*, 2000, **100**, 105-109.

2 H. Yoshinaga, Y. Arami, O. Kajita and T. Sakai, *J. Alloys Compd.*, 2002, **330**, 846-850.

3 C. H. Hare and S. J. Wright, *J. Coat. Technol.*, 1982, **54**, 65-76.

4 A. S. Oliver, *USP-3539114*, 1970.

5 S. P. Wu, R. Y. Gao and L. H. Xu, *J. Mater. Process. Technol.*, 2009, **209**, 1129-1133.

6 R. Zhang, W. Lin, K. Lawrence and C. P. Wong, *Int. J. Adhes. Adhes.*, 2010, **30**, 403-407.

7 L. Zheng, B. Cui, N. G. Akdogan, W. Li and G. C. Hadjipanayis, *J. Alloys Compd.*, 2010, **504**, 391-394.

8 X. Wang, R. Gong, P. Li, L. Liu and W. Cheng, *Mater. Sci. Eng., A.*, 2007, **466**, 178-182.

9 S. Wu, *J Mater SCI-Mater EL.*, 2006, **18**, 447-452.

10 R. Schmid and N. Mronga, *USP-5624486*, 1997.

11 P. Pal, S. K. Pahari, A. Sinhamahapatra, A. K. Giri, H. C. Bajaj and A. B. Panda, *RSC Adv.*, 2013, **3**, 2802-2811.

12 L. S. Fu, J. T. Jiang and C. Y. Xu, *CrystEngComm.*, 2012, **14**, 6827-6832.

13 Y. Liu, L. Chen and J. Hu, *J. Phys. Chem. C.*, 2010, **114**, 1641-1645.

14 D. T. Hurd and E. G. Rochow, *J. Am. Chem. Soc.*, 1945, **67**, 1057-1059.

15 W. J. Ward, A. Ritzer and K. M. Carroll, *J. Catal.*, 1986, **100**, 240-249.

16 J. M. Bablin, A. C. Crawford and D. C. Demoulpied, *Ind. Eng. Chem. Res.*, 2003, **42**, 3555-3565.

17 L. N. Lewis, W. V. Ligon and J. C. Carnahan, *Silicon Chem.*, 2002, **1**, 23-33.

18 N. Floquet, S. Yilmaz and J. L. Falconer, *J. Catal.*, 1994, **148**, 348-368.

19 L. N. Lewis and W. J. Ward, *Ind. Eng. Chem. Res.*, 2002, **41**, 397-402.

This journal is © The Royal Society of Chemistry 2014

20 J. M. Bablin, L. N. Lewis and P. Bui, *Ind. Eng. Chem. Res.*, 2003, **42**, 3532-3543.

21 D. H. Sun, B. E. Bent, A. P. Wright and B. M. Naasz, *J. Mol. Catal. A: Chem.*, 1998, **131**, 169-183.

22 T. J. Wessel and D. G. Rethwisch, *J. Catal.*, 1996, **161**, 861-866.

23 H. H. Don, J. D. Ronald and P. S. George, *USP-4503165*, 1985.

24 L. D. Gasper-Galvin, D. M. Sevenich, H. B. Friedrich and D. G. Rethwisch, *J. Catal.*, 1991, **128**, 468-478.

25 Y. Zhu, Y. Wang, L. Song, X. Chen, W. Liu, J. Sun, X. She, Z. Zhong and F. Su, *RSC Adv.*, 2013, **3**, 9794-9802.

26 J. P. Kim and D. G. Rethwisch, *J. Catal.*, 1992, **134**, 168-178.

27 Z. Zhang, H. Che, Y. Wang, X. She, J. Sun, P. Gunawan, Z. Zhong and F. Su, *ACS Appl. Mater. Interfaces.*, 2012, **4**, 1295-1302.

28 Z. Zhang, H. Che, Y. Wang, J. Gao, L. Zhao, X. She, J. Sun, P. Gunawan, Z. Zhong and F. Su, *Ind. Eng. Chem. Res.*, 2012, **51**, 1264-1274.

29 Z. Zhang, H. Che, J. Gao, Y. Wang, X. She, J. Sun, P. Gunawan, Z. Zhong and F. Su, *Catal. Sci. Technol.*, 2012, **2**, 1207-1212.

30 Z. Zhang, H. Che, Y. Wang, L. Song, Z. Zhong and F. Su, *Catal. Sci. Technol.*, 2012, **2**, 1953-1960.

31 Z. Zhang, H. Che, Y. Wang, J. Gao, X. She, J. Sun, Z. Zhong and F. Su, *RSC Adv.*, 2012, **2**, 2254-2256.

32 X. Chen, L. Jia, Y. Wang, L. Song, Y. Zhu, W. Liu, Z. Zhong and F. Su, *J. Colloid Interface Sci.*, 2013, **404**, 16-23.

33 Z. Zhang, H. Che, Y. Wang, J. Gao, Y. Ping, Z. Zhong and F. Su, *Chem. Eng. J.*, 2012,

This journal is © The Royal Society of Chemistry 2014

211-212, 421-431.

34 W. Liu, L. Jia, Y. Wang, L. Song, Y. Zhu, X. Chen, Z. Zhong and F. Su, *Ind. Eng. Chem. Res.*, 2013, **52**, 6662-6668.

35 L. Lu and Y. F. Zhang, *J. Alloys Compd.*, 1999, **290**, 279-283.

36 Y. Wang, J. Yang, C. Ye, X. Fang and L. Zhang, *Nanotechnology.*, 2004, **15**, 1437-1440.

37 Z. Han, L. Lu, H. W. Zhang, Z. Q. Yang, F. H. Wang and K. Lu, *Oxid. Met.*, 2005, **63**, 261-275.

38 M. Yin, C. K. Wu and Y. Lou, *J. Am. Chem. Soc.*, 2005, **127**, 9506-9511.

39 R. Vijaya Kumar, R. Elgamiel and Y. Diamant, *Langmuir.*, 2001, **17**, 1406-1410.

40 J. A. Rodriguez, J. Y. Kim and J. C. Hanson, *Catal. Lett.*, 2003, **85**, 247-254.

41 G. M. Raynaud and R. A. Rapp, *Oxid. Met.*, 1984, **21**, 89-102.

42 T. N. Rhodin Jr, *J. Am. Chem. Soc.*, 1950, **72**, 5102-5106.

43 J. H. Park and K. Natesan, *Oxid. Met.*, 1993, **39**, 411-435.

44 G. R. Wallwork and W. W. Smeltzer, *Corrosion Sci.*, 1969, **9**, 561-563.

45 H. Souha, E. Gaffet and F. Bernard, *J. Mater. Sci.*, 2000, **35**, 3221-3226.

46 D. H. Sun, B. E. Bent and A. P. Wright, *Catal. Lett.*, 1997, **46**, 127-132.

This journal is © The Royal Society of Chemistry 2014

Table Caption:

Table 1 The physical parameters of all the samples.

Table 2 Catalytic performance of all the catalysts for Rochow reaction.

Figure Captions:

Fig. 1 XRD patterns (a), TG curves (b), H_2-TPR curves (c), and PSD curves (d) of all the samples.

Fig. 2 SEM images of Cu (a and b), Cu-f (c and d), CuO-Cu_2O-f (e and f), CuO-Cu_2O-Cu-f (g and h), CuO-CuO-f (i and j), and CuO-f (k and l).

Fig. 3 TEM images of Cu-f (a), Cu-Cu_2O-f (b), Cu-Cu_2O-CuO-f (c), Cu_2O-CuO-f (d), and CuO-f (e).

Fig. 4 Schematic illustration of the oxidation reaction process of Cu flakes.

Fig. 5 XRD patterns of waste contact masses (a) and enlarged view in the 2θ range of 40–50^o (b).

Fig. 6 SEM images of Si particle after reaction (a), elemental mapping images of Si (b), Cu (c), and schematic illustration of the Rochow reaction process (d).

This journal is © The Royal Society of Chemistry 2014

Table 1

Sample	Cu[a] (nm)	Cu_2O[a] (nm)	CuO[a] (nm)	Cu[b] (wt %)	Cu_2O[b] (wt %)	CuO[b] (wt %)	T_M[c] (^oC)	S_{TPR}[d]	Particle size[e] (μm)
Cu	32.5	0.0	0.0	100.0	0.0	0.0	————	————	31.2
Cu-f	28.9	0.0	0.0	100.0	0.0	0.0	————	————	21.7
Cu-Cu_2O-f	28.5	28.3	0.0	53.0	47.0	0.0	389.9	6959.6	20.7
Cu-Cu_2O-CuO-f	28.0	34.3	38.3	27.9	40.9	31.2	387.7	14348.3	20.4
Cu_2O-CuO-f	0.0	39.7	45.1	0.0	39.1	60.9	380.1	22017.9	20.2
CuO-f	0.0	0.0	54.7	0.0	0.0	100.0	376.3	26662.5	17.5

[a] The grain size of Cu, Cu_2O,and CuO of all samples calculated from the XRD patterns.

[b] The weight percent of Cu, Cu_2O, and CuO determined by oxidimetry.

[c] Temperatures at the peak maximum from H_2-TPR patterns.

[d] The hydrogen consumption peak area of samples from H_2-TPR patterns.

[e] The particle size value of the catalysts from laser particle analyzer.

This journal is © The Royal Society of Chemistry 2014

Table 2

Sample	Product Composition（%）							C-Si (%)
	M1	M2	M3	M1H	M2H	LB	HB	
Cu-p	67.6	5.7	1.9	22.5	0.1	0.7	1.5	1.6
Cu-f	26.7	54.0	2.9	12.1	0.3	0.6	3.4	16.3
Cu-Cu_2O-f	23.5	62.5	1.8	10.3	0.5	0.7	0.7	24.8
Cu-Cu_2O-CuO-f ^{1st}	10.2	82.0	1.9	4.4	0.6	0.3	0.6	32.4
Cu-Cu_2O-CuO-f ^{2nd}	10.3	82.3	1.7	4.2	0.6	0.3	0.6	32.5
Cu-Cu_2O-CuO-f ^{3rd}	10.9	81.8	1.5	4.1	0.7	0.3	0.7	32.1
Cu_2O-CuO-f	10.5	80.1	1.6	6.2	0.7	0.3	0.6	30.7
CuO-f	10.9	78.4	1.2	7.8	0.7	0.3	0.7	28.3

This journal is © The Royal Society of Chemistry 2014

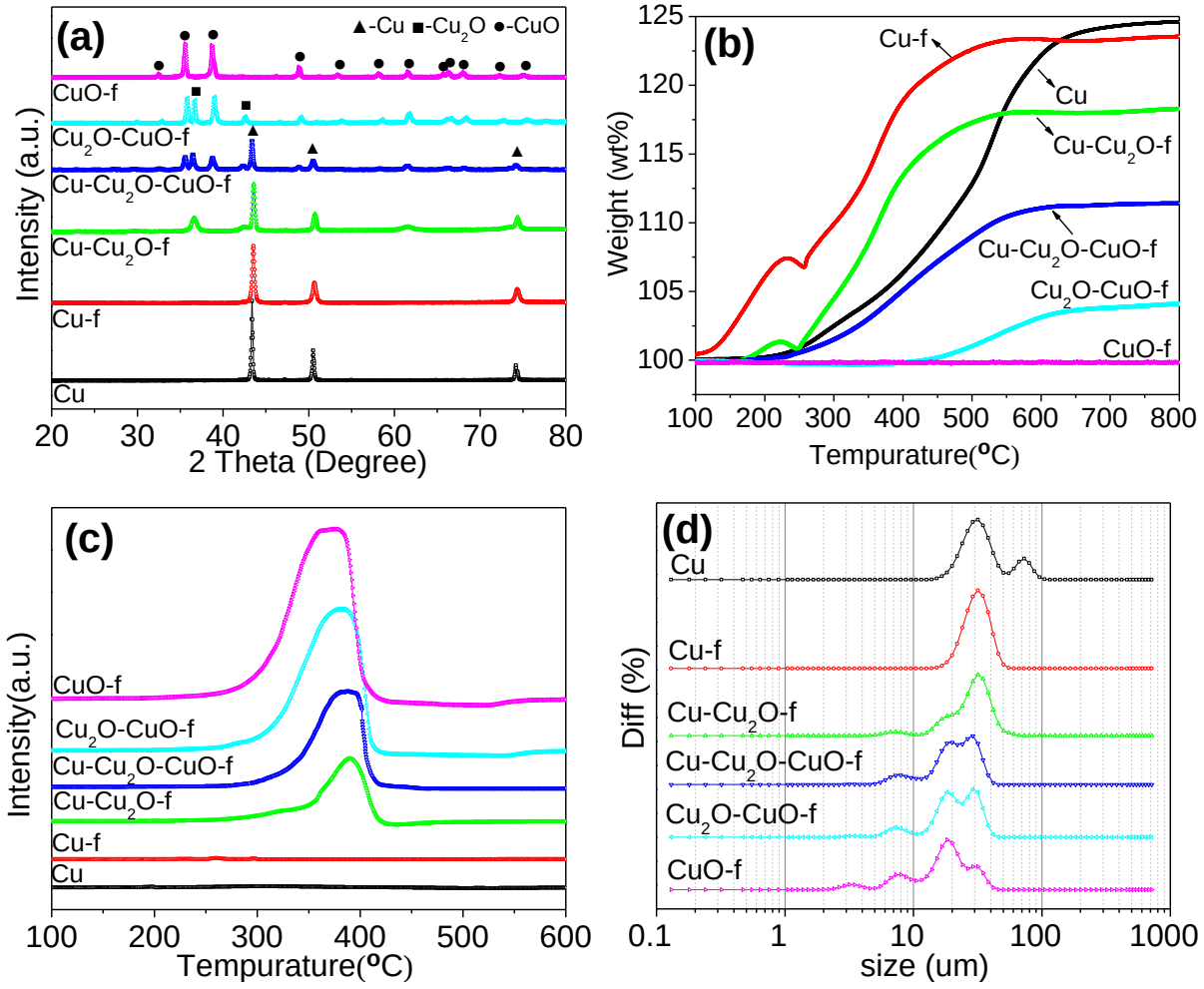

Fig. 1

This journal is © The Royal Society of Chemistry 2014

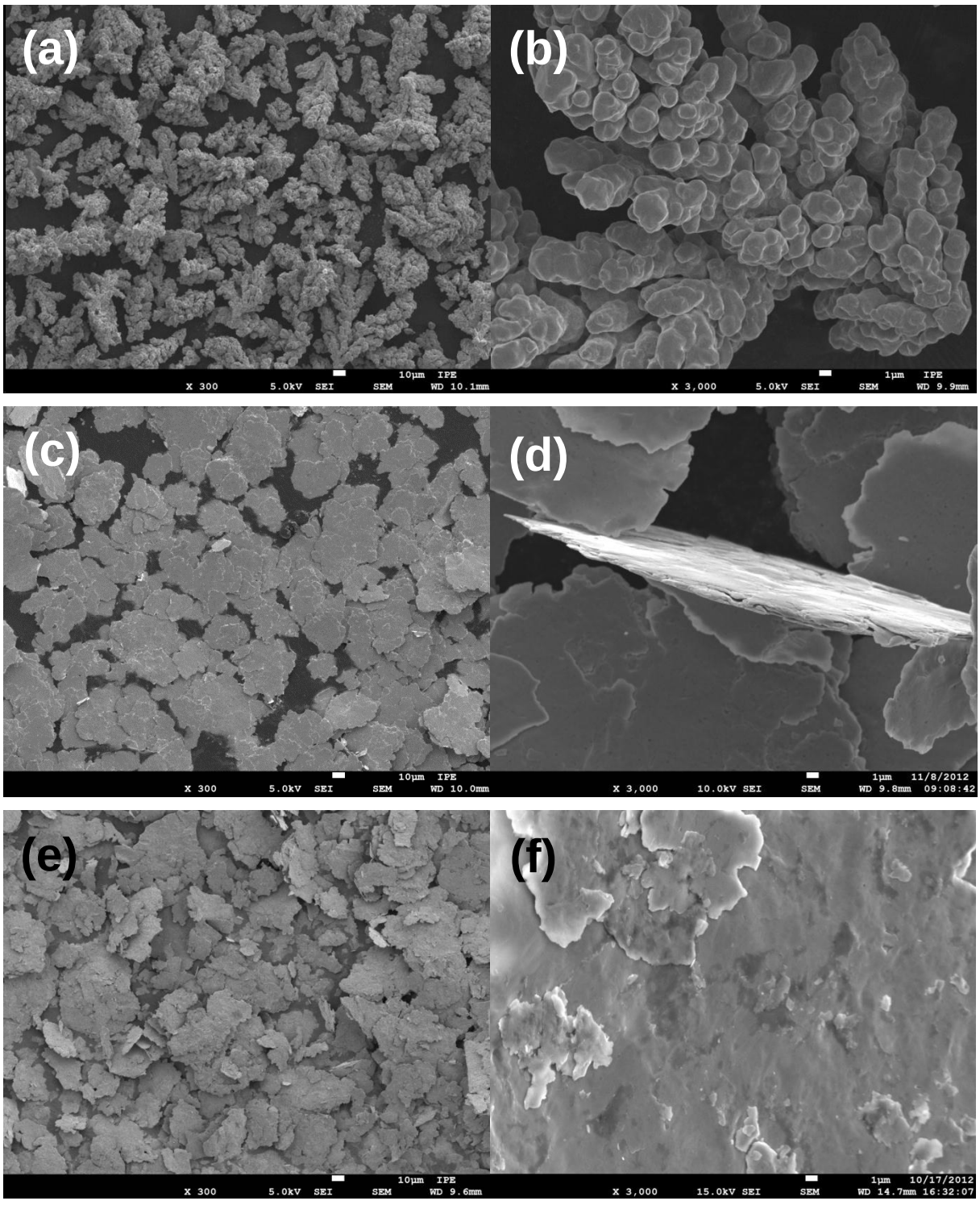

This journal is © The Royal Society of Chemistry 2014

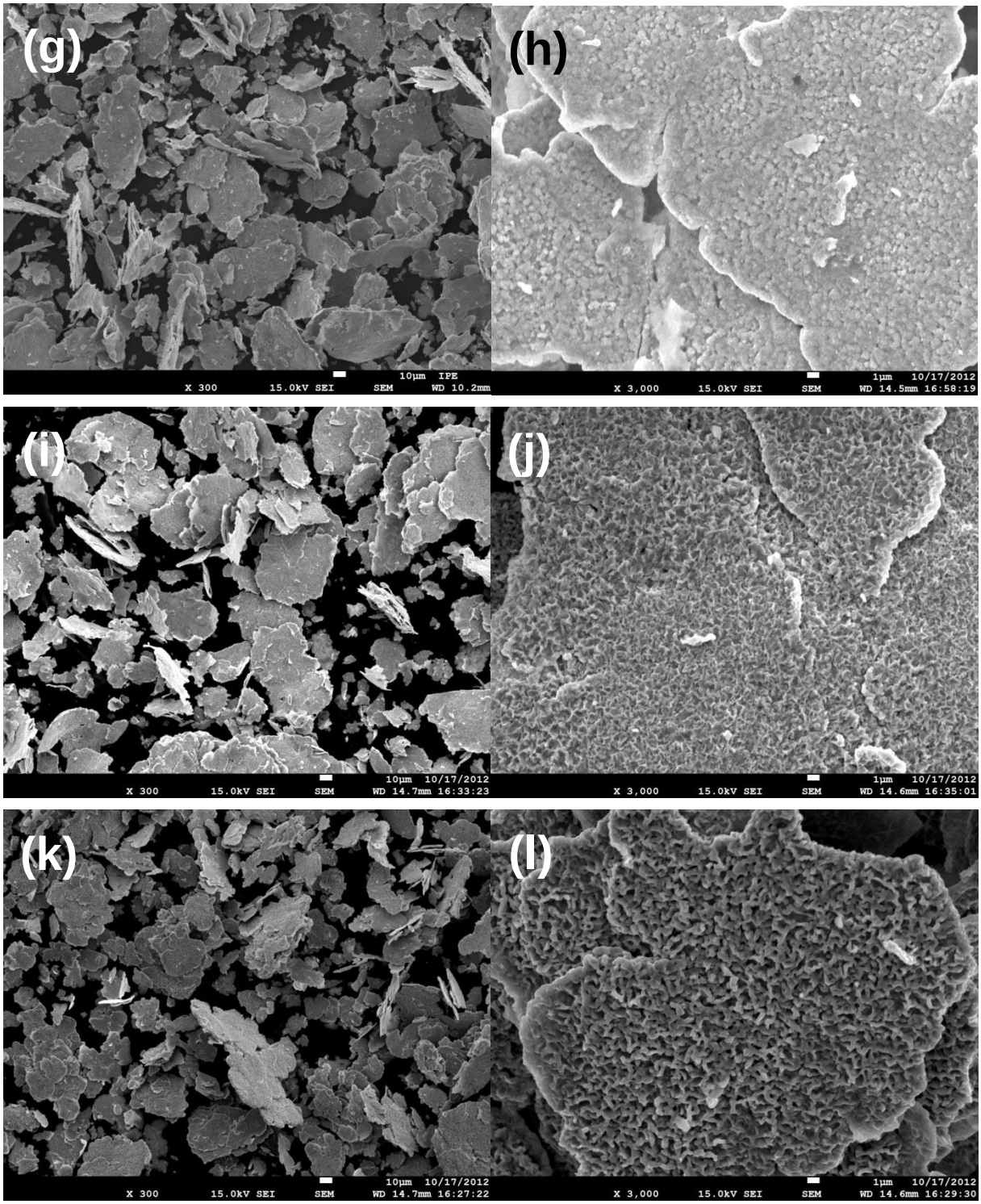

Fig. 2

This journal is © The Royal Society of Chemistry 2014

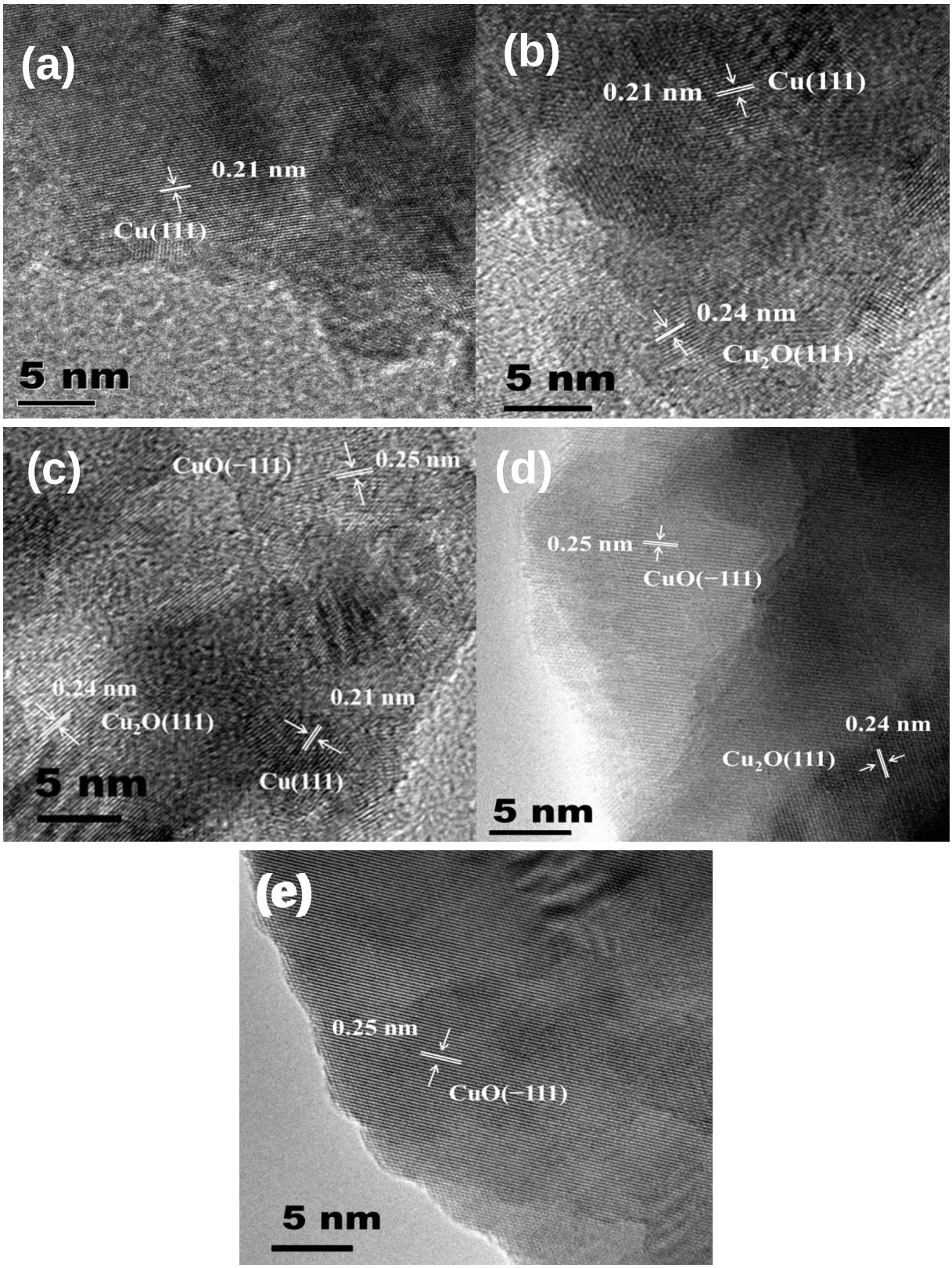

Fig. 3

This journal is © The Royal Society of Chemistry 2014

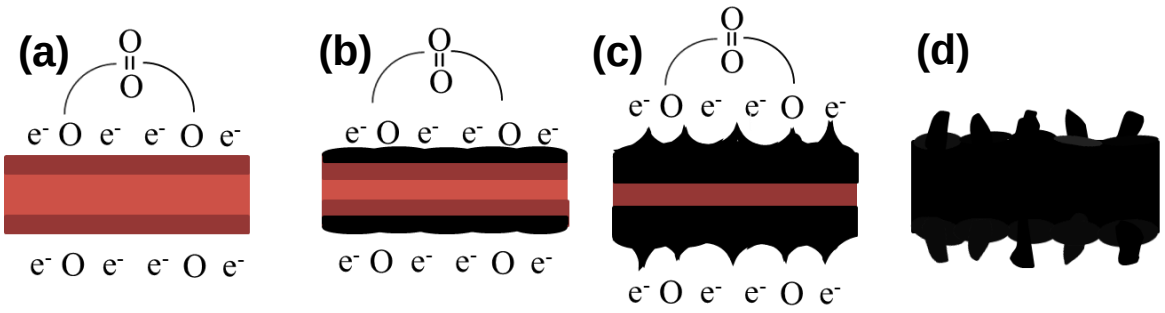

Fig. 4

This journal is © The Royal Society of Chemistry 2014

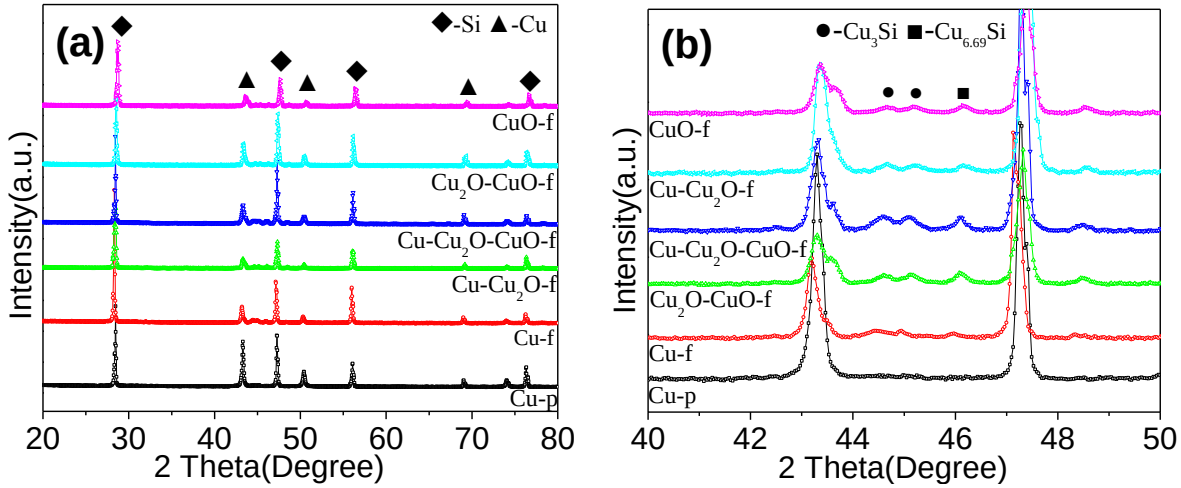

Fig. 5.

This journal is © The Royal Society of Chemistry 2014

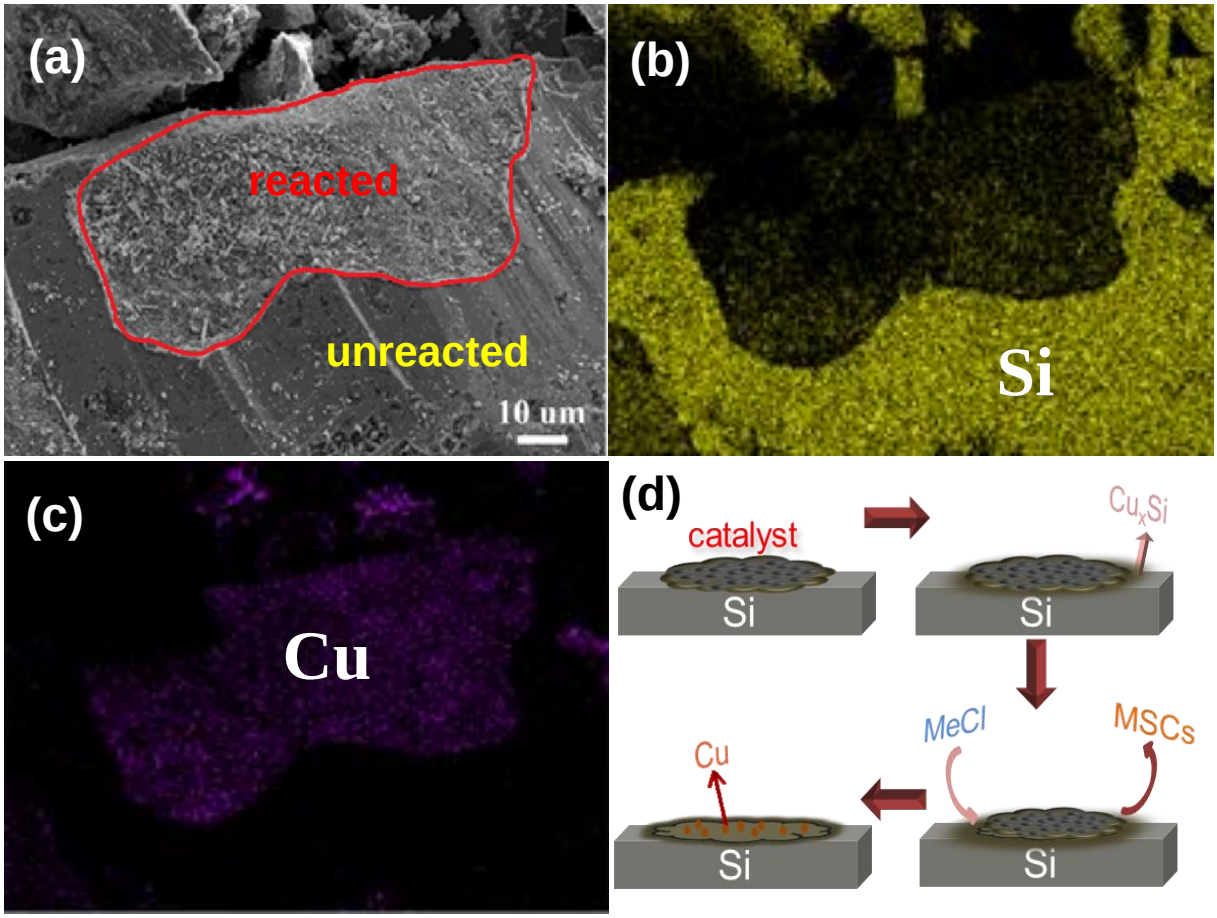

Fig. 6